Additive Manufacturing Letters 8 (2024) 100188

Contents lists available at ScienceDirect

Additive Manufacturing Letters

journal homepage: www.elsevier.com/locate/addlet

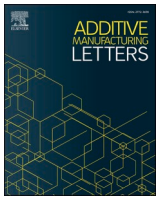

Short Communication

High-speed direct energy deposition as a high-throughput design tool for laser-based additive manufacturing

Klaus Büßenschütt [a,*], Patrick Köhnen [b], Fabian Kies [c], Stephan Koß [a], Johannes Henrich Schleifenbaum [a], Christian Haase [c]

[a] Digital Additive Production, RWTH Aachen University, 52072 Aachen, Germany
[b] GKN Powder Metallurgy Engineering GmbH, 53177 Bonn, Germany
[c] Steel Institute, RWTH Aachen University, 52072 Aachen, Germany

ARTICLE INFO

Keywords:
Additive manufacturing
Extreme high-speed laser material application
Laser powder bed fusion
Direct energy deposition
Solidification
Rapid alloy development

ABSTRACT

A wide range of additive manufacturing (AM) processing conditions can be rapidly realized within a single specimen via high-speed direct energy deposition laser based (DED-LB), due to a variety of cooling conditions and in-situ powder mixing. Since existing approaches are inefficient in exploring the vast material and process design space in AM, high-speed DED-LB can be employed as a novel technology for high-throughput alloy design tool. However, an evaluation of the process transferability of the high-speed DED-LB process with respect to the currently dominating metal AM technologies, namely laser powder bed fusion (PBF LB/M) and conventional DED-LB, is required. In this study, high-speed DED-LB is applied for the high-throughput sample production, using the nickel alloy IN718 as reference material as well as the AM processes PBF LB/M and DED-LB as reference processes. The resulting microstructures are characterized and compared using optical microscopy and large-area scanning electron microscopy (SEM) analysis combined with energy-dispersive X-ray spectroscopy (EDS). Furthermore, a model for calculation of the volumetric energy density is developed to compare the applied AM processes. The significant influence of the processing conditions on the solidification behavior of the investigated material allows for efficient exploration of the microstructure and phase composition. Specific high-speed DED-LB-process conditions achieved the average solidification cell size and laves phase content as observed in the PBF LB/M- and DED-LB -produced counterparts. The applicability of the high-speed DED-LB process for rapid alloy and process development, i.e., process transferability, is critically evaluated. The results show that high-speed DED-LB can be used to emulate cooling conditions of PBF-LB/M and DED-LB and, therefore, be used as tool for rapid alloy development.

1. Introduction

Additive manufacturing (AM) is now one of the most promising technologies for CO_2-free and individualized production of high-performance components [6]. In fact, the highest growth rates in the upcoming years are predicted for AM of metallic materials [24]. Although AM machines have now reached a high industrial maturity, there is a severe lack of metals and alloys available. Amongst the few alloys for AM, there is an even smaller fraction that has been designed explicitly for AM, whereas the majority are materials that were originally designed for conventional processing routes [2,9,20]. The key to achieve desired properties and performances of AM components is to fine-tune the combination of processing conditions and the material's chemistry to yield tailored microstructures. This can be reached via controlling the cooling conditions and solidification behavior [13]. However, the high dimensionality of the chemistry- process parameter space makes traditional alloy development strategies inapplicable. Additionally, the production of raw materials via powder atomization is energy-intensive and inflexible, making the use of powder blends necessary [3]. Consequently, a sufficient rapid alloy development (RAD) process needs to allow for the flexibility of chemical composition, sufficient mixing of elemental powders and a short development time.

The most widely used metal AM process is laser powder bed fusion (PBF LB/M) [4]. In PBF LB/M, the powder is distributed layer wise in the building chamber and selectively molten [18]. The deflection of the laser through a mirror enables very high process speeds, resulting in

* Corresponding author.
E-mail address: klaus.buessenschuett@dap.rwth-aachen.de (K. Büßenschütt).

https://doi.org/10.1016/j.addlet.2023.100188
Received 26 September 2023; Received in revised form 21 November 2023; Accepted 30 November 2023
Available online 2 December 2023

Table 1
Selected HS-DED process parameter combinations.

Primary HS-DED parameter	Laser power	Track displacement	Process speed	Powder mass flow	Carrier Ar gas flow	Shielding Ar gas flow	Laser spot diameter
HS-DED-slow	1000 W	0.35 mm/rev	5 m/min	ca. 7 g/min	14 l/min	14 l/min	1.2 mm
HS-DED-fast	2400 W	0.15 mm/rev	100 m/min	ca.24 g/min	14 l/min	14 l/min	1.2 mm

typical cooling rates of 10^6 – 10^7 K/s [10,18]. It enables a higher degree of geometrical freedom and reduces material waste, in comparison to direct energy deposition laser based (DED-LB) [1]. Ewald et al. [3] and Kies et al. [12] investigated PBF LB/M of powder blends as alloy development tool for high entropy alloys (HEA) and advanced high-strength steels (AHSS) and showed the sufficient mixing of elemental powders in the resulting component. Despite this success, the chemical composition cannot be varied during a PBF LB/M build job. Developing alloys with PBF LB/M is, therefore, slow and lacks flexibility [3]. Additionally, the use of elements with highly different melting points and/or particle sizes can lead to inhomogeneous chemical composition [11].

Laser based direct energy deposition (DED-LB) is a nozzle-based AM process, where the powder is fed into the process and molten layer-wise on the surface of the substrate [17]. The typical cooling rates are in the range of 10^2 to 10^4 K/s [16]. In comparison to PBF LB/M, DED-LB offers the opportunity to repair and modify components by depositing metal on their surface [7]. Additionally, the process allows to change the chemical composition of the deposited powder in-situ [8]. Haase et al. [8] developed a successful method to use DED-LB in combination with computational screening as alloy development tool for HEAs. Nevertheless, the disadvantages of the process by means of alloy development are the limited geometrical flexibility and the high tendency to form process-induced defects, as compared to PBF LB/M [5]. A new high-speed DED-LB process, called extreme high-speed laser application (further referred to as HS-DED for differentiation to conventional DED-LB, developed by RWTH Aachen University and the Fraunhofer-Institute for Laser Technology ILT, Germany) was developed to overcome the shortcoming of PBF LB/M and DED-LB mentioned above. HS-DED is also a DED process, in which, in comparison to DED-LB, the melting of the powder is independent from the melt pool. This is implemented by a shift of the powder focus above the surface of the specimen [21]. This modification allows high process speeds of up to 200 m/min [19] and mixing of powders independently from melt pool kinetics and segregation processes [15]. The envisioned advantages are the homogeneous mixing of elemental powders in the process and the possibility of high-throughput sample production.

Since the cooling rates in DED-LB and PBF LB/M vary strongly, the resulting microstructures of metallic materials, e.g. Inconel 718 (IN718), show severe differences in terms of the solidification cell size, phase fractions and defects [22,25]. Consequently, designing new alloys for either PBF LB/M or DED-LB requires to mimic the respective process conditions precisely. The HS-DED process covers a wide range of cooling rates, adaptable through different process parameters, especially the process speed [15]. This study investigates the feasibility of the HS-DED process as a fast and flexible tool to emulate the PBF LB/M and DED-LB conditions. Therefore, IN718 samples are produced with different process conditions, covering the full variety of cooling rates in HS-DED. The samples are characterized using light optical microscopy, large-area SEM, and EDS to identify process-microstructure correlations. The envisioned method will rapidly increase the alloy development efficiency and will provide deeper insights into process-material interactions in AM.

2. Materials and methods

2.1. Sample fabrication by HS-DED

17 HS-DED specimens for microstructure analysis were produced (laser power: 1000 W to 2400 W, process speed: 5 to 125 m/min, powder mass flow: 7 to 24 g/min) using a Hornet HS-DED system (Hornet Laser Cladding BV, Netherlands). The 4-axis handling system has a tiltable turning spindle to process rotationally symmetrical components with dimensions up to Ø 250 × 500 mm. The rotation speed can reach up to 1300 rpm. The laser beam source was a TruDisc4002 disk laser (Trumpf GmbH + Co. KG., Germany) with a wavelength of 1030 nm and maximum output power of 4 kW. Steel tubes (seamless precision steel tubes E355+C (St52-BK) EN 10305-1 / DIN 2391) were used as substrate cylinders. Two layers of individual tracks, 7 mm in width, were deposited on top of each other on the substrate cylinder using the HS-DED process. Two of the 17 produced process parameter combinations were selected (

Table 1) based on the similarity of microstructural features with DED-LB and PBF LB/M conditions. The PBF-LB/M samples were produced using the Aconity MINI PBF-LB/M system (Aconity 3D GmbH, Herzogenrath). A 10 × 10 × 10 mm^3 cube was produced on a steel (ST37) substrate. The DED-LB samples were produced on a MODULO 400 (AddUp GmbH, Aachen). On a steel substrate plate (St52) a sample with 30 tracks and 60 layers was deposited. The total samples size was 30 × 30 × 30 mm^3. The process parameter combinations of the IN718 DED-LB and PBF LB/M processes are given in Table 2.

A schematic figure of the HS-DED process with the essential process parameters is shown in Fig. 1 and Table 1. The process parameters that influence the energy input into the powder particles and the substrate material are the particle velocity $v_{particle}$ and the powder mass flow $\dot{m}_p$ in the powder gas stream. As $\dot{m}_p$ increases, the energy absorption per powder particle decreases. This results in reduced heating of the particles. An increased carrier gas flow V_{CG} leads to an increased $v_{particle}$ and reduced interaction time with the laser beam, reducing the heating of individual particles. The energy input into the substrate is mainly influenced by process speed v_p and track displacement f, by which the track overlap can be controlled. With increasing v_p, the interaction time between the laser beam and the substrate decreases, reducing energy input into the substrate. This leads to a reduction in melt pool size and the size of the heat-affected zone. Furthermore, the processing speed can be used to influence the cooling rate of the layers produced. An increase in the processing speed increases the cooling speed [15].

Table 2
DED-LB and PBF LB/M process parameter combinations.

Primary DED parameter	Laser power	Track displacement	Process speed	Powder mass flow	Carrier Ar gas flow	Shielding Ar gas flow	Laser spot diameter
DED-LB	1500 W	1 mm	2 m/min	ca. 18 g/min	6 l/min	10 l/min	2 mm
Primary PBF LB/M parameter		Laser power	Hatch distance	Laser speed	Layer thickness	Laser spot diameter	
PBF LB/M		285 W	0.007 mm	60 m/min	0.003 mm	0.08 mm	

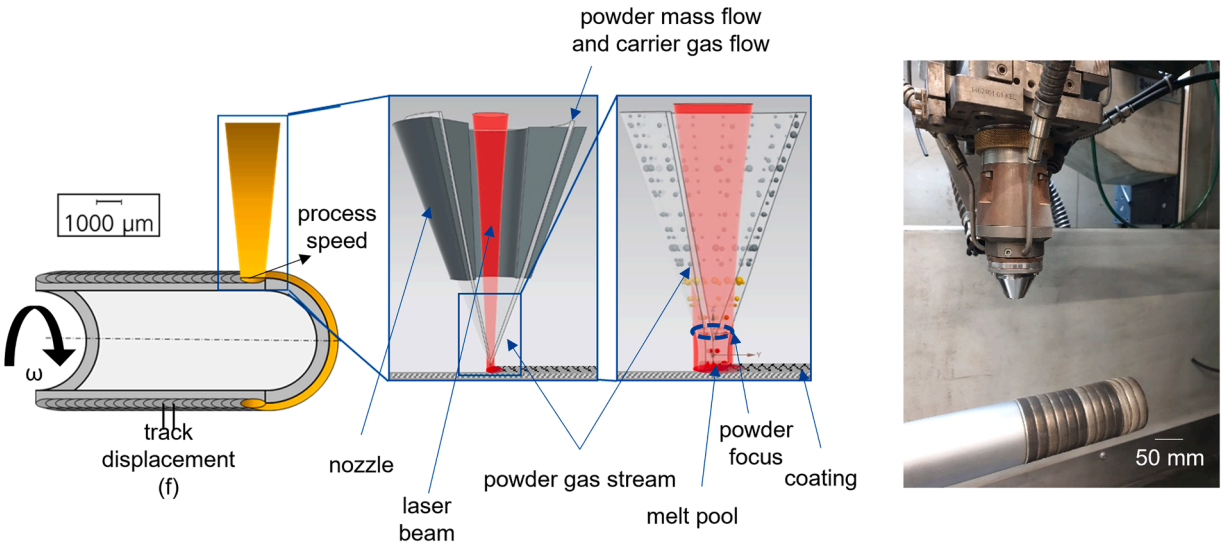

Fig. 1. Schematic illustration of the extreme high-speed laser application (HS-DED) process (left). IN718 powder deposited by a nozzle on a rotating substrate cylinder with varying rotation speed (5 – 100 m/min) using a laser beam with varying laser powder (1000 – 2400 W) (right).

Table 3
Chemical composition of IN718 argon gas atomized metal powder. C was measured by the combustion method. All other elements were measured by ICP-OES. All contents are given in wt. %.

Ni	Cr	Nb	Mo	Ti	Co	Al	Fe	C
balance	18.25	5.44	3.04	0.93	0.34	0.52	17.8	0.02

2.2. Materials

The IN718 powder (provided by EOS GmbH, Germany) is argon gas atomized using the EIGA (Electrode Induction Melting Gas Atomization) technique. The chemical composition of the powder is given in Table 3. The powder particles revealed a spheroidal shape, were sieved and air separated to ensure a size distribution between 15-45 µm. The particle size volume distributions (Fig. 2) were measured by optical image analysis according to ISO 13322-2 using a Camsizer X2 particle analyzer (Retch Technology GmbH, Germany).

2.3. Sample preparation

Microstructural characterization was conducted on the cross-section of the substrate cylinder and the HS-DED deposited material. The specimens were prepared for LOM analysis by mechanical cutting, mechanical grinding (up to 1200 SiC grit paper), mechanical polishing (3 and 1 µm diamond suspension) and etching with V2A etchant for 30-45 seconds. For SEM/EDS, after mechanical polishing, the samples were electro-polished with a LectroPol-5 electrolytic polishing device (Struers GmbH, Germany) using an A2 electrolyte (Struers GmbH, Germany) for 15 s at 26 V at room temperature.

2.4. Microstructure characterization

For melt pool characterization, a VHX6000 LOM (Keyence Deutschland GmbH, Germany) was used. The melt pools were measured, and the aspect ratio calculated. Since the heat conductivity of IN718 is low (~11.4 W/Ks), heat accumulates during the building process and melt-pools expand with increasing height. Therefore, all measurements were taken from melt-pools starting at around 150 - 250 µm building height. The height was measured parallel and the width perpendicular to the building direction. For microstructural analyses, a field emission

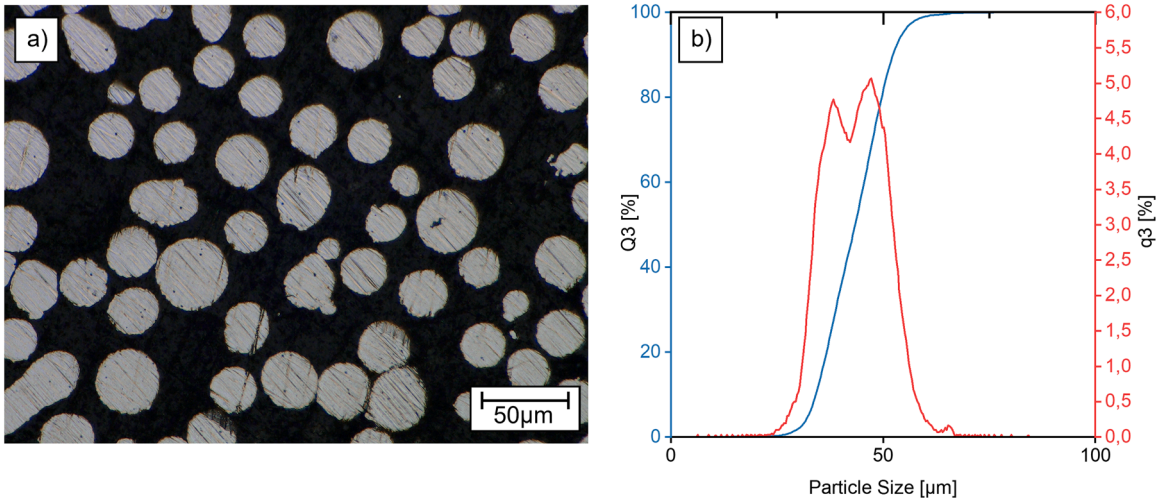

Fig. 2. (a) Optical micrograph and (b) cumulative (Q3) and differential (q3) particle size distribution of the IN718 powder used in this study.

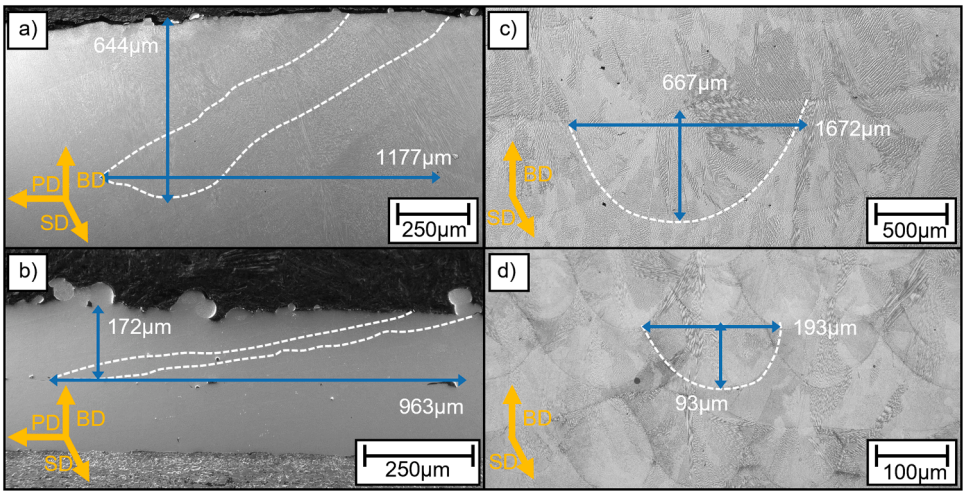

Fig. 3. Melt pool dimensions for a) HS-DED$_s$, b) HS-DED$_f$, c) DED-LB and d) PBF LB/M samples, BD = building direction, SD = scanning direction, PD = process direction.

gun SEM (Carl Zeiss AG, Germany) was used with secondary electrons (SE), back scatter electrons (BSE) and X-Max 50 EDS detectors (Oxford Instruments PLC, UK). Combined SE, BSE, and EDS measurements were used to identify the average solidification cell size, laves phase content, and elemental segregation. Average solidification cell size was calculated using the line intercept method. BSE data were processed and analyzed with a custom watershed image processing algorithm using MATLAB (Mathworks Inc., USA) to derive laves phase contents.

2.5. Process parameter comparison

To compare the different AM processes, theoretical models to calculate the volumetric energy density (E_V) for the different processes were developed based on the laser material interaction during the processes.

3. Results and discussion

The aim of this work was to verify HS-DED as an emulator for the AM processes DED-LB and PBF LB/M. Therefore, correlations between the process conditions and microstructures of IN718 samples manufactured by the aforementioned AM processes have been identified.

3.1. Melt pool characterization

The different melt pool dimensions are shown in Fig. 3. The HS-DED melt pools show the typical elongated melt pool morphology in process direction. The melt pools of the sample produced at lowest speed (HS-DED$_s$) already show a pronounced elongated structure in process direction. The aspect ratio of the melt pool (depth / width) for HS-DED$_s$ is 0.54. When increasing the process speed, the width of the melt pool does not change significantly, but the height decreases. For the HS-DED samples produced at highest speed (HS-DED$_f$), the height is only 26 % of the height of the HS-DED$_s$ melt pool. Consequently, the aspect ratio decreases to 0.18. The elongation of the melt pools and the resulting low aspect ratio can be justified by the energy input of the process. During HS-DED, the main fraction of laser energy (~80 %) is absorbed by the powder, which is then deposited on the previous layer as a molten film. Only a small fraction of laser power (~20 %) is introduced into the previous layer or the substrate [15]. The deposited powder forms a molten film, rather than a melt pool with molten substrate or previous layer. Therefore, the molten film is deposited on top of the previous track with almost no remelting. In combination with the high overlap of the melt tracks in the HS-DED process, these molten film morphologies occur. This heat conduction welding has typically aspect ratios below 0.5 and the molten films are influenced by laser power, process speed and conductivity of the material. The increased process speed will increase the width and decrease the height of the molten film. The smaller track displacement for HS-DED$_f$ in this study suppresses the width increase, whereas the depth decrease is still significant. If, in contrast to HS-DED, the powder melting and melt pool formation are not independent, the melt pool characteristics change. The DED-LB and PBF LB/M melt pools show a nearly symmetric, curved geometry. The aspect ratios of the DED-LB and PBF LB/M melt pools are 0.4 and 0.48, respectively. Although DED-LB and PBF LB/M are often defined as deep penetration welding techniques (aspect ratio > 0.5), the process parameters chosen in this study show similar depths in HS-DED melt pools, as in DED-LB and PBF LB/M, but with completely different morphologies. The melt pool of HS-DED$_s$ and DED-LB, as well as HS-DED$_f$ and PBF LB/M are similar in depth.

3.2. Process parameter comparison

To compare the different processes, different models to calculate the volumetric energy density E_V are modified and combined. The standard PBF LB/M model is given by Eq. (1) [18].

$$E_{V,\mathrm{PBF\ LB\ /\ M}} = \frac{P_L}{D_S * v_p * \Delta y_S} \tag{1}$$

with P_L = laser power, D_S = layer thickness, v_p = process speed, Δy_S = hatch distance.

With Eq. (1), E_V describes the laser energy per build-up volume, which allows for comparing the influence of different process parameters in PBF LB/M on E_V. Furthermore, remelting of already deposited material is of high importance for the resulting microstructure. If a single melt pool is observed, the first melting of the powder is described by Eq. (1). Additionally, the melt pool experiences cyclic remelting due to neighboring tracks and following layers. This is not taken into account in Eq. (1). Therefor the overlap is divided from the calculated built-up volume in the denominator of Eq. (1). To include the remelting by the following layers, the layer thickness is determined by the measured melt pool depths, since D_s used for the PBF-LB/M sample, is more than twice smaller than the actual measured melt pool depth. The resulting Eq. (2) for PBF LB/M and DED-LB is defined as follows.

$$E_{V,\mathrm{PBF\ LB/M\ /\ DED-LB}} = \frac{P_L * (1+f)}{D_{MP} * v_p * \Delta y_S} \tag{2}$$

Table 4
Volumetric Energy Density (E_V) for DED, PBF LB/M and HS-DED.

Process	E_V [J/mm^3]
DED	101.2
PBF LB/M	49,25 *(Equ.1: 133,6)*
HS-DED$_s$	98.6
HS-DED$_f$	76.3

with f = track overlap, D_{MP} = melt pool depth.

For HS-DED, there are two major assumptions to derive the E_V parameter. First, the laser power is mostly absorbed by the powder particles midair and not by the melt pool. Therefore, the approximation of Koß et al. is taken to calculate E_V based on the powder density and powder mass flow, as given in Eq. (3) [15].

$$E_{V,EHLA\ powder} = \frac{P_L * \rho_{Mat}}{\dot{m}_p} \quad (3)$$

ρ_{Mat} and $\dot{m}_p$ denote the material density and powder mass flow, respectively.

Second, it is assumed that 80 % of the laser power is absorbed by the powder particles, whereas 20 % is absorbed by the melt pool. This results in the following Eq. (4) for calculation of E_V for the HS-DED process.

$$E_{V,EHLA} = 0,8 * E_{V,EHLA\ powder} + 0,2 * E_{V,\text{PBF LB/M / DED–LB}} \quad (4)$$

The resulting values are summarized in Table 4. It can be seen that the values are ranging from ~ 50 J/mm^3 to ~ 100 J/mm^3. The DED-LB E_V is higher than the PBF LB/M value. When using the standard calculation for E_V in PBF LB/M, the accounting layer thickness would only be D_S, whereas the heat input influences the previous layers as well. Accordingly, the value calculated using Eq. (1) is much higher (133,6 J/mm^3) than the one (49,25 J/mm^3) calculated using Eq. (2). These results are in agreement with previous studies on the E_V of PBF LB/M for high manganese steels [15]. The resulting DED-LB and HS-DED$_s$ values are close to each other, whereas the value for PBF LB/M is 25 J/mm^3 lower than the value for HS-DED$_f$. Since E_V is used in PBF LB/M to compare processes with different materials, it can be assumed that a similar value will result in similar solidification behavior in DED-LB and HS-DED$_s$. This hypothesis is evaluated by microstructure analysis in Sections 3.3 and 3.4.

3.3. HS-DED microstructures

The microstructures of all produced HS-DED samples (Fig. 4) show the typical AM microstructure of IN718 with fine columnar grains in building direction (BD). Epitaxial grain growth results in a strong elongation in [001]-direction parallel to the AM building direction. It is noticeable, that the process speed in HS-DED has an impact on the cell size of the HS-DED samples. The solidification cell size vertical to the BD for HS-DED$_s$, with 2.86 µm, is around three times larger than the size of the HS-DED$_f$ samples with 1.00 µm (Table 5). This decrease in size with process speed is typical for AM microstructures. Due to the faster process speed, the cooling rate increases. This results in smaller grain and solidification cell sizes [23]. The EDX line scans were performed perpendicular to the cell elongation direction along the colored lines in Fig. 4. It can be seen that the process speed has an influence on the Nb distribution. Nb segregates interdendritic and is enriched between the dendrites at the end of solidification [1]. Consequently, the peaks of Nb are around three times wider separated in HS-DED$_s$ than in HS-DED$_f$, confirming the above-mentioned solidification cell size difference. Additionally, the Nb content in the interdendritic regions decreases with increasing process speed. In the HS-DED$_s$ samples, 10 - 22 % Nb are present in between the solidification cells, whereas in HS-DED$_f$ only 7 – 12 % Nb are observed. Chen et al. investigated an inverse relation between the cooling rate and the Nb-segregation of the Laves Phase. With fast cooling rates, the time for diffusion is short, resulting in low Nb-concentrations in the Laves phase. Since the cooling time decreases with increasing cooling rate, the segregation of Nb is more pronounced at lower cooling rates [1] and thus, more pronounced in HS-DED$_s$. Since the main strengthening phase in IN718 γ“ has the stoichiometric composition Ni_3Nb, the precipitation hardening inside the grains can be decreased by Nb segregation [14]. HS-DED$_f$ has less Nb-segregations than HS-DED$_s$. Consequently, an increasing process speed of HS-DED can increase the possible γ’’-fraction after heat treatment.

Table 5
Comparison of microstructural features.

Additive manufacturing process	Average solidification cell size (µm)	Laves phase content (area %)
DED	2.97	3.32
HS-DEDs	2.86	3.47
HS-DED$_f$	1.00	10.10
PBF LB/M	1.01	8.35

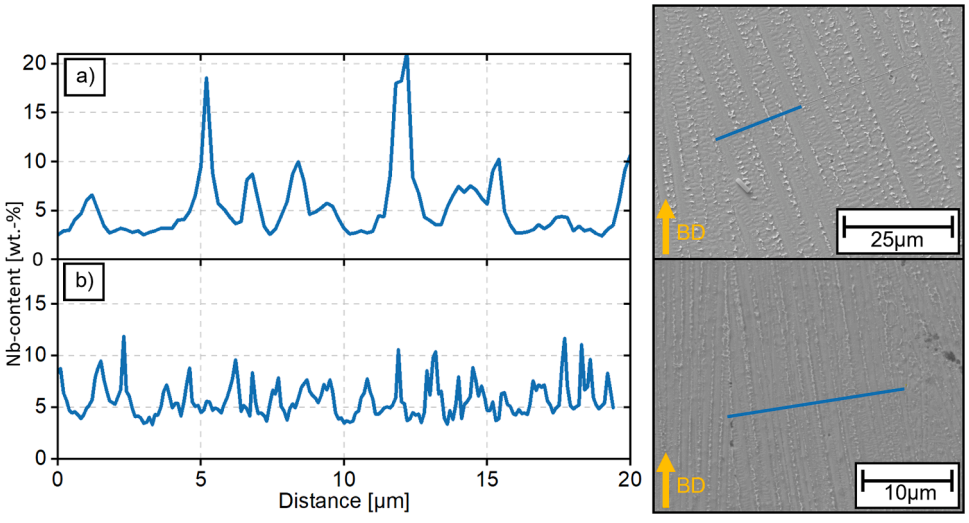

Fig. 4. EDX Line scans for a) HS-DED$_s$ and b) HS-DED$_f$.

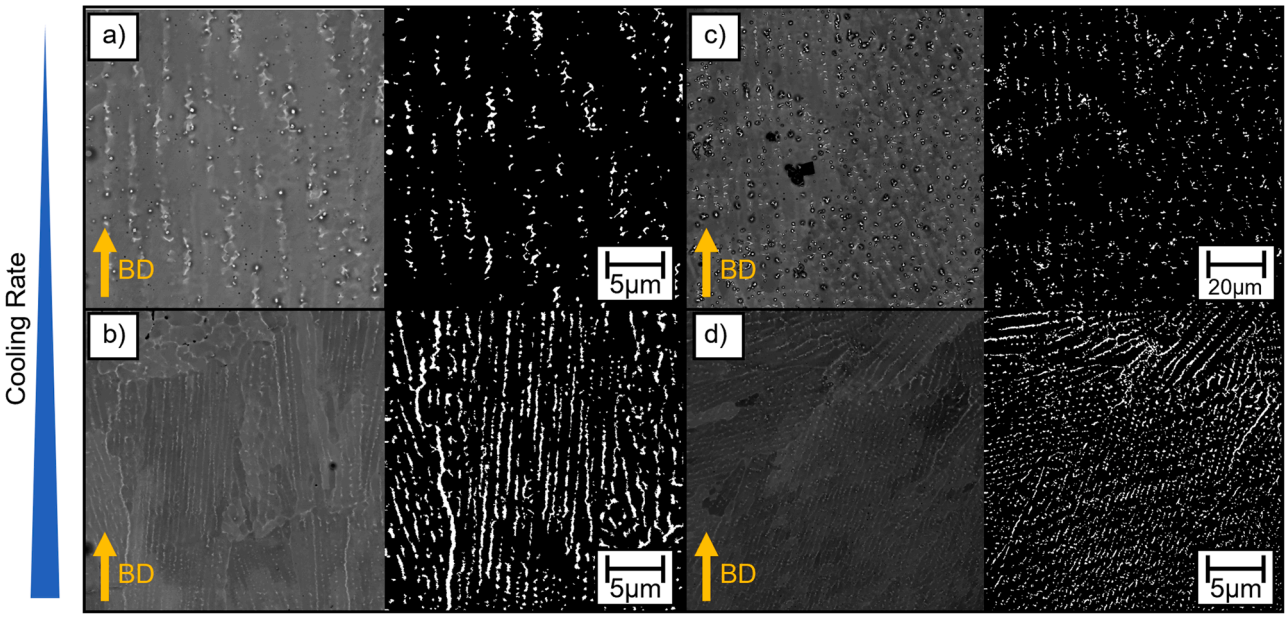

Fig. 5. BSE and corresponding analyzed BSE micrograph for (a) HS-DED$_s$, (b) HS-DED$_f$, (c) DED and (d) PBF LB/M. White areas in the analyzed BSE micrographs reveal the Laves phase.

3.4. Comparison with DED and PBF LB/M

The microstructures of the DED and PBF LB/M samples (Fig. 5 c and d) show the typical elongation of fine columnar grains in building direction. Comparing the DED and HS-DED$_s$ samples, the microstructure appears similar. With 2.97 µm the solidification cell size (Table 5) perpendicular to the BD of the DED sample is similar to the one of the HS-DED$_s$ sample. Fig. 5 shows the Laves phase in the different samples in the analyzed BSE graphs. An increasing Laves phase content with increasing cooling rate can be identified. The Laves phase of DED and HS-DED$_s$ has a similar morphology. It forms interdendritic in disrupted islands in both samples. The fraction of Laves phase, as shown in Table 5, is with 3.47 % in HS-DED$_s$ similar to the fraction of the DED sample with 3.32 %. In HS-DED$_f$, the share of Laves phase increased to 10.10 %. The morphology changes from disrupted islands to complete films on the cell boundaries. This morphology can also be seen in the PBF LB/M sample. The fraction in the PBF LB/M sample is with 8.35 % slightly lower than in the HS-DED$_f$ sample.

The results show that the HS-DED process can be used, to mimic DED and PBF LB/M processes for IN718. The theoretical E_V models showed similar values for HS-DED$_s$ and DED, as well as HS-DED$_f$ and PBF LB/M. The resulting microstructures regarding the solidification cell size, Laves phase content and morphology also reveal this correlation. The cooling rate is validated to have the main influence on the microstructure and can be used to connect the different processes. For rapid alloy development, the proposed method enables fast screening of a wide alloy space and has the potential to accelerate the development process.

4. Conclusions

High-throughput HS-DED sample production and alloy characterization were used to explore the microstructure evolution of additively manufactured IN718 in comparison with established DED and PBF LB/M techniques. The following conclusions can be drawn:

- Cooling and solidification conditions of the HS-DED process are highly adjustable by changing process speed and laser power.
- The E_V can be determined by the developed theoretical model for all three processes and allows for comparability based on process parameters and melt pool size for HS-DED$_s$ and DED.
- It is possible to mimic/reproduce microstructural aspects such as cell size and Laves phase composition as in IN718 processed by standard AM techniques, i.e., DED-LB and PBF LB/M.
- HS-DED has the potential to serve as a rapid screening technology for accelerated material and process development for established metal AM processes.

CRediT authorship contribution statement

Klaus Büßenschütt: Conceptualization, Methodology, Formal analysis, Writing – original draft, Visualization. **Patrick Köhnen:** Conceptualization, Methodology, Writing – original draft. **Fabian Kies:** Investigation, Writing – original draft. **Stephan Koß:** Investigation, Writing – original draft. **Johannes Henrich Schleifenbaum:** Resources, Funding acquisition, Writing – review & editing, Supervision. **Christian Haase:** Conceptualization, Methodology, Funding acquisition, Writing – review & editing, Supervision.

Declaration of Competing Interest

The authors declare that they have no known competing financial interests or personal relationships that could have appeared to influence the work reported in this paper

Data availability

Data will be made available on request.

Acknowledgment

This research is funded by the Digital Photonic Production DPP Research Campus as part of the "Research Campus Public-Private Partnership for Innovation" research funding initiative of the German Federal Ministry of Education and Research (BMBF). As part of the German government's high-tech strategy, the BMBF is using this initiative to promote strategic and long-term cooperation between science and industry "under one roof" (project ID: 13N15423). Additionally funded by the Deutsche Forschungsgemeinschaft (DFG, German Research Foundation) under Germany´ s Excellence Strategy – EXC-2023 Internet of

Production – 390621612. CH also acknowledges the support of the BMBF within the NanoMatFutur project “MatAM - Design of additively manufactured high-performance alloys for automotive applications” (project ID: 03XP0264).

References

[1] Yuan Chen, Ke Zhang, Jian Huang, Seyed Reza Elmi Hosseini, Zhuguo Li, Characterization of heat affected zone liquation cracking in laser additive manufacturing of Inconel 718, Mater. Design 90 (2016) 586–594, https://doi.org/10.1016/j.matdes.2015.10.155.

[2] T. DebRoy, H.L. Wei, J.S. Zuback, T. Mukherjee, J.W. Elmer, J.O. Milewski, et al., Additive manufacturing of metallic components – Process, structure and properties, Prog. Mater Sci. 92 (2018) 112–224, https://doi.org/10.1016/j.pmatsci.2017.10.001.

[3] Simon Ewald, Fabian Kies, Steffen Hermsen, Maximilian Voshage, Christian Haase, Johannes Henrich Schleifenbaum, Rapid alloy development of extremely high-alloyed metals using powder blends in laser powder bed fusion, Materials (Basel, Switzerland) 12 (10) (2019), https://doi.org/10.3390/ma12101706.

[4] Simon; Ford, Mélanie Despeisse, Additive manufacturing and sustainability: an exploratory study of the advantages and challenges, J. Cleaner Prod. 137 (2016) 1573–1587, https://doi.org/10.1016/j.jclepro.2016.04.150.

[5] Andres Gasser, Gerhard Backes, Ingomar Kelbassa, Andreas Weisheit, Konrad Wissenbach, Laser additive manufacturing, LTJ 7 (2) (2010) 58–63, https://doi.org/10.1002/latj.201090029.

[6] Ian Gibson, David Rosen, Brent Stucker, Additive Manufacturing Technologies, Springer New York, New York, NY, 2015.

[7] Benjamin; Graf, Andrey; Gumenyuk, Michael Rethmeier, Laser metal deposition as repair technology for stainless steel and titanium alloys, Phys. Procedia 39 (2012) 376–381, https://doi.org/10.1016/j.phpro.2012.10.051.

[8] Christian; Haase, Florian; Tang, Markus B. Wilms, Andreas; Weisheit, Bengt Hallstedt, Combining thermodynamic modeling and 3D printing of elemental powder blends for high-throughput investigation of high-entropy alloys – towards rapid alloy screening and design, Mater. Sci. Eng. A (688) (2017) 180–189, https://doi.org/10.1016/j.msea.2017.01.099.

[9] Dirk Herzog, Vanessa Seyda, Eric Wycisk, Claus Emmelmann, Additive manufacturing of metals, in: Acta Mater., 117, 2016, pp. 371–392, https://doi.org/10.1016/j.actamat.2016.07.019.

[10] Paul A. Hooper, Melt pool temperature and cooling rates in laser powder bed fusion, Additive Manuf. 22 (2018) 548–559, https://doi.org/10.1016/j.addma.2018.05.032.

[11] Yaqing Hou, Hang Su, Hao Zhang, Xuandong Wang, Changchang Wang, Fabricating homogeneous FeCoCrNi high-entropy alloys via SLM in situ alloying, Metals 11 (6) (2021) 942, https://doi.org/10.3390/met11060942.

[12] Fabian Kies, Patrick Köhnen, Markus B. Wilms, Frederike Brasche, Konda G. Pradeep, Alexander Schwedt, et al., Design of high-manganese steels for additive manufacturing applications with energy-absorption functionality, Mater. Design 160 (2018) 1250–1264, https://doi.org/10.1016/j.matdes.2018.10.051.

[13] Patrick Köhnen, Simon Ewald, Johannes Henrich Schleifenbaum, Andrey Belyakov, Christian Haase, Controlling microstructure and mechanical properties of additively manufactured high-strength steels by tailored solidification, in: Addit. Manuf., 35, 2020, 101389, https://doi.org/10.1016/j.addma.2020.101389.

[14] Mageshwari Komarasamy, Shivakant Shukla, Sarah Williams, Kumar Kandasamy, Shawn Kelly, Rajiv S Mishra, Microstructure, fatigue, and impact toughness properties of additively manufactured nickel alloy 718, in: Addit. Manuf., 28, 2019, pp. 661–675, https://doi.org/10.1016/j.addma.2019.06.009.

[15] Stephan Koß, Simon Ewald, Marie-Noemi Bold, Jan Hendrik Koch, Maximilian Voshage, Stephan Ziegler, Johannes Henrich Schleifenbaum, Comparison of the EHLA and LPBF process in context of new alloy design methods for LPBF, AMR 1161 (2021) 13–25, https://doi.org/10.4028/www.scientific.net/AMR.1161.13.

[16] Fa-yun Lu, Hong-yuan Wan, Xin Ren, Li-ming Huang, Hai-lin Liu, Xin Yi, Mechanical and microstructural characterization of additive manufactured Inconel 718 alloy by selective laser melting and laser metal deposition, J. Iron Steel Res. Int. 29 (8) (2022) 1322–1333, https://doi.org/10.1007/s42243-022-00755-x.

[17] Rasheedat Modupe Mahamood, Laser Metal Deposition Process of Metals, Alloys, and Composite Materials, Springer International Publishing, Cham, 2018. Engineering Materials and Processes SerAvailable online at, https://ebookcentral.proquest.com/lib/kxp/detail.action?docID=5024553.

[18] Wilhelm Meiners, Dissertation. RWTH, Aachen. Lehrstuhl für Lasertechnik, 1999.

[19] N. Pirch, S. Linnenbrink, A. Gasser, K. Wissenbach, R. Poprawe, Analysis of track formation during laser metal deposition, J. Laser Appl. 29 (2) (2017) 22506, https://doi.org/10.2351/1.4983231.

[20] Behrang Poorganji, Eric Ott, Rajandra Kelkar, Andrew Wessman, Mahdi Jamshidinia, Review: materials ecosystem for additive manufacturing powder bed fusion processes, JOM 72 (1) (2020) 561–576, https://doi.org/10.1007/s11837-019-03892-z.

[21] Thomas Schopphoven, Andres Gasser, Gerhard Backes, EHLA: extreme high-speed laser material deposition, LTJ 14 (4) (2017) 26–29, https://doi.org/10.1002/latj.201700020.

[22] Itziar Serrano-Munoz, Tobias Fritsch, Tatiana Mishurova, Anton Trofimov, Daniel Apel, Alexander Ulbricht, et al., On the interplay of microstructure and residual stress in LPBF IN718, J. Mater. Sci. 56 (9) (2021) 5845–5867, https://doi.org/10.1007/s10853-020-05553-y.

[23] Hong-ying Wang, Bin-bin Wang, Liang Wang, Ran Cui, Liang-shun Luo, Yan-qing Su, Impact of laser scanning speed on microstructure and mechanical properties of Inconel 718 alloys by selective laser melting, in: China Foundry, 18, 2021, pp. 170–179, https://doi.org/10.1007/s41230-021-9011-7.

[24] Terry Wohlers, Robert Ian Campbell, Olaf Diegel, Joseph Kowen, Noah Mostow, Wohlers Report 2021. 3D Printing and Additive Manufacturing: Global State of the Industry, Wohlers Associates, Fort Collins, Colorado, 2021.

[25] Kangbo Yuan, Weiguo Guo, Penghui Li, Jianjun Wang, Yu Su, Xin Lin, Yanping Li, Influence of process parameters and heat treatments on the microstructures and dynamic mechanical behaviors of Inconel 718 superalloy manufactured by laser metal deposition, Mater. Sci. Eng. A (721) (2018) 215–225, https://doi.org/10.1016/j.msea.2018.02.014.